Carbon 142 (2019) 300–310

Contents lists available at ScienceDirect

Carbon

journal homepage: www.elsevier.com/locate/carbon

Uncertainty analysis and estimation of robust AIREBO parameters for graphene

Gurjot Dhaliwal [a], Prasanth B. Nair [b], Chandra Veer Singh [a, c, *]

[a] Department of Mechanical and Industrial Engineering, University of Toronto, Toronto, ON, M5S 3G8, Canada
[b] Institute of Aerospace Studies, University of Toronto, Toronto, ON, M3H 5T6, Canada
[c] Department of Materials Science and Engineering, University of Toronto, Toronto, ON, M5S 3E4, Canada

ARTICLE INFO

Article history:
Received 23 June 2018
Received in revised form
4 October 2018
Accepted 5 October 2018
Available online 9 October 2018

ABSTRACT

AIREBO is one of the commonly utilized interatomic potential (IP) for performing molecular dynamics (MD) simulations of graphene and carbon nanostructures. With its parameters fitted to a limited dataset, property prediction outside of the original training set can be challenging and can lead to uncertainty in the predicted values. This is especially important for 2D materials such as graphene which have limited experimental data and have widely varying predicted properties in the literature. In this study, we conducted a comprehensive Uncertainty Quantification (UQ) analysis of AIREBO potential parameters and their corresponding effect on the predicted properties of graphene. We found that computed output properties were highly sensitive to small variations in IP parameters. For instance, a 0.5% change in IP parameters led to a 66% change in the predicted elastic constants. Based on our UQ analysis, we developed a new robust IP parameter set for the AIREBO potential with significantly reduced sensitivity towards output properties. The robust parameters were derived using a Markov Chain Monte Carlo scheme, considering gaussian noise in available DFT data. We were also able to obtain realistic error bars on MD predictions by using posterior probability distributions and propagating the underlying variance to the final properties.

1. Introduction

Molecular Dynamics (MD) simulations play an increasingly key role in understanding the structure-property relationships of nanomaterials such as graphene and carbon nanostructures. MD simulations utilize interatomic potential (IP) energy functions that are mathematically fitted to a set of quantum chemistry and experimental property data. Numerous IP functions which address specific types of substances or properties have been created. The same IP is often used to simulate a variety of disparate properties varying form thermal conductivity to mechanical elasticity or chemical reactivity for the same material.

Modern MD simulations generally rely on many body potentials which can have dozens of adjustable parameters required to be fitted to data. This has led to increasing interest in uncertainty quantification (UQ) of MD simulation predictions [1–3]. UQ can be crucial for simulations of 2D materials which are difficult to test experimentally and whose impressive properties are often predicted based on MD simulations. Graphene, which shows commercial potential in diverse areas such as battery anodes, gas and bio-sensors, field effect transistors [4–9], is a prime example of a material extensively studied through MD simulations. The AIREBO potential, developed by Stuart et al. [10], is one of the most commonly utilized IP to simulate graphene and carbon nanostructures. Originally created for hydrocarbons, the AIREBO potential is fitted to a relatively old, structure-property database involving density functional theory (DFT) or experimental values for substances such as graphite and methane (but not including graphene).

As an example of the difficulty in obtaining predictive values for graphene, the experimental and simulation results for mechanical properties of graphene contain huge variation [11–13]. Variation specific to atomistic models has been observed for DFT versus MD values for C_{12} of graphene where DFT predicts its value to be 65 N/m [14] while MD studies predict it to be 98 N/m [15]. Depending on the input parameters, surface states and disorders, unusual

* Corresponding author. Department of Mechanical and Industrial Engineering, University of Toronto, Toronto, ON, M5S 3G8, Canada.
E-mail addresses: gurjot.dhaliwal@mail.utoronto.ca (G. Dhaliwal), pbn@utias.utoronto.ca (P.B. Nair), chandraveer.singh@utoronto.ca (C.V. Singh).

https://doi.org/10.1016/j.carbon.2018.10.020
0008-6223/

transport properties are predicted [16]. In light of these highly varying predictions and limited experimental data for graphene, it is critical to perform UQ [17,18] for the MD simulation models parameters.

Studies have indicated that parameterization of these IP functions has been a cause of transferability issues [19,20]. Fittings of these parameters are based on the most likely value which gives little information about distribution of the parameters itself. If the most likely value is the Maximum a Posteriori (MAP) value, it can lead to significant overfitting. Thus, a critical question arises: How do the final properties of interest change with variation in the IP parameters from MAP estimate? And how much variation can be expected in these parameters? In other words, what is the probability distribution of these parameters given the experimental observations. Answers to these questions are critical as it has been shown in earlier works that the final properties are sensitive to the changes in the IP parameters [21–26]. Even the simple Lennard-Jones potential with only two parameters revealed very high sensitivity towards free energy values for amino acids and CS_2 [21–23]. As a first application of Bayesian methods to this problem, Frederiksen et al. [27] compared the performance of an ensemble of IP, given the uncertainty in the corresponding IP parameters and propagated this uncertainty to the final predictions. The work in Refs. [28,29] applied similar ideas to different material systems. Parameter calibration through inverse Bayesian methods has also been addressed for simpler models like water [30] and argon systems [31] where number of IP parameters was less than 4. Further investigations to address this problem have been carried for a water system [32,33] and metals [34] and a critical review can be found at [35]. Most of the work in IP parameter sensitivity and parameter calibration has involved simple potentials like Lennard-Jones with number of parameters less than 4. More complex IP functions with more than 4 parameters, such as AIREBO, have not been considered in previous studies. Apart from the requirement of developing algorithms capable of dealing with high-dimensional parameter spaces, appropriate noise models reflecting the high uncertainty in the experimental observations of graphene are also required.

In order to address the high-dimensional parameter space UQ of AIREBO potential for graphene applications, we developed a framework that can be used to (i) assess the sensitivity of various Quantities of Interest (QOI) with respect to the IP parameters, (ii) obtain probability distributions of the IP parameters which are robust towards experimental values of QOI, and (iii) propagate the underlying IP parameter uncertainty to the corresponding prediction of QOI. We assessed the sensitivity of AIREBO by first analyzing the variation of predicted QOI with respect to its parameters. Using the generated dataset as prior, we used a gaussian likelihood model to assess the posterior probability distribution of the IP parameters. Posterior distributions were approximated through a Markov Chain Monte Carlo (MCMC) sampling algorithm. The sampled posterior probability distributions denote the uncertainty in the IP parameters or potential energy surfaces which is propagated to final QOI by performing MD simulations or through surrogate models. The uncertainty in experimental observations was captured through gaussian noise models. Using this information, we were able to obtain realistic error bars on MD predictions. The sampled posterior distribution was used to develop a new parameter set for the AIREBO potential (using the latest DFT simulation data) which display less sensitive QOI than the original parameters.

2. Methodology

2.1. Molecular dynamics

The core of any MD study is the IP function, the function that dictates the interatomic interactions. In this work, we studied the parameter sensitivity of a special IP function for hydrocarbons, the AIREBO potential. Fittings for the AIREBO potential are performed on a structure-property database involving DFT/experiment values for hydrocarbons like graphite and methane. The energy equation for the AIREBO potential can be written as

$$E = E^{REBO} + E^{LJ} + E^{Tors}, \tag{1}$$

where E^{REBO} is the covalent bonding interactions from REBO potential, E^{LJ} is the Lennard-Jones (LJ) term and E^{Tors} is the term compensating for the torsional interactions. Each of the terms has a definite functional form, details of which can be found in Ref. [10]. As the material of our choice is graphene, we will be focusing only on the parameters with Carbon–Carbon interactions.

MD simulations were performed using the open source software LAMMPS [36]. As shown in Fig. 1, a simulation cell with number of atoms corresponding to each QOI was designed. In the middle of the simulation cell, one layer of graphite was created with a lattice constant of 2.46 A^o. With rest of the volume as vacuum, this layer of graphite atoms resembles graphene. The structure of the graphene is confirmed by visualizations in Ovito [37] and by comparison of the radial distribution function to the ones available from previous studies [38]. Another check to confirm the graphene structure is carried out by comparing the basic properties computed using LAMMPS such as the cohesive energy and lattice constant to the experimental, MD and DFT results of graphene from the literature. Once the structure is confirmed, simulations for higher-order properties like elastic constants and defect formation energies were performed. Further, details on the simulation setup are documented in supporting information, SI 1. Table 1 presents the comparison of each QOI to the corresponding experimental values and first principles calculations from other studies in the literature. The phonon frequency at τ point for LO branch is denoted by while ω_2 denotes the phonon frequency at same point for TO branch.

2.2. Parametric constraints

As mentioned in equation (1), AIREBO can be visualized as sum of REBO potential, LJ potential and Torsional term. UQ analysis in the original parameter space can be computationally challenging. To ease the computations, relationships between different parameters are introduced using physical assumptions. While fitting the parameters for Stillinger-Webb based IP for MoS_2, similar assumptions were employed [57].

2.2.1. REBO parameters

The REBO potential assumes the following form

$$V(r_{ij}) = V_{repulsion} - b_{ij} V_{attraction}. \tag{2}$$

The repulsion part of the potential, $V_{repulsion}$, and attraction part of the potential, $V_{attraction}$, can be written as

$$V_{repulsion} = f_{cut}(r_{ij}) A \exp(-\alpha r_{ij}) [1 + (Q/r_{ij})] \tag{3}$$

and

$$V_{attraction} = f_{cut}(r_{ij}) \sum_{n=1,3} B_{IJn} \exp\left(- \beta_{IJn} r_{ij} \right), \tag{4}$$

where $f_{cut}(r_{ij})$ is the smooth cutoff function [58]. The term connecting the repulsion and attraction part of the potential energy function is the term bond order, denoted by b_{ij}. In Ref. [58], fittings for this potential are done in two stages. Values for the pair

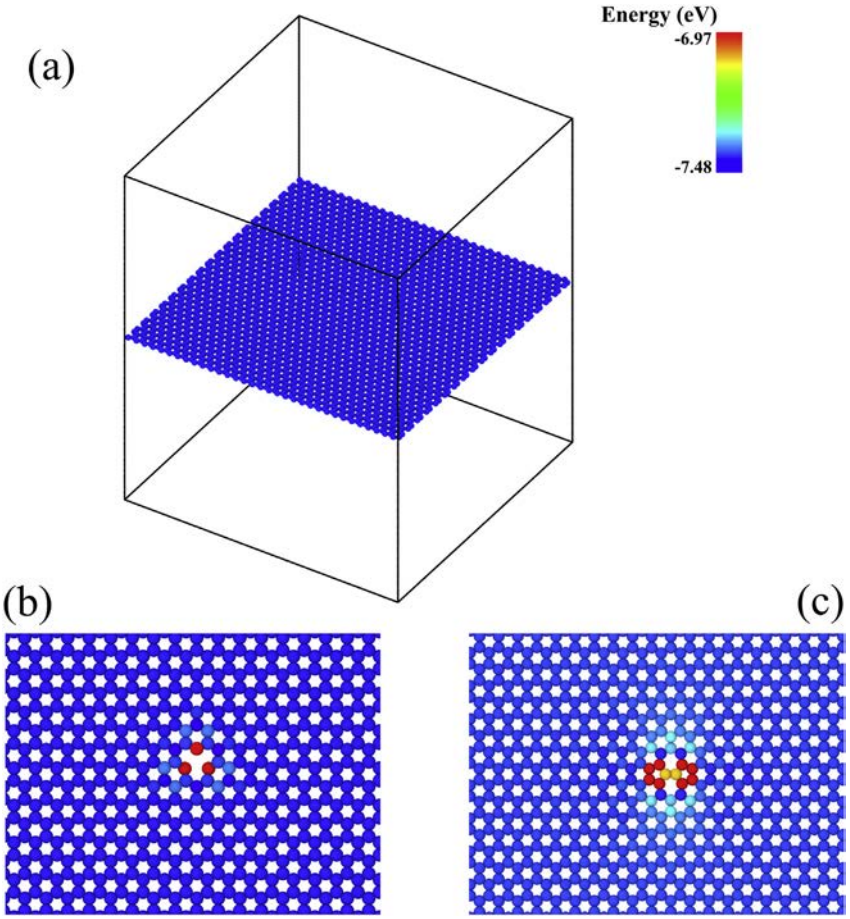

Fig. 1. (a) Simulation cell containing Graphene sheet. Atoms are color coded with the corresponding energy values. At ground state, each atom is having −7.46 eV (cohesive) of energy. Energy perturbations occur in the presence of defects. A single vacancy defect is shown in Fig. 1(b). With a single missing atom three 5 atom rings are formed with atoms having high energy (colored red). Figure (c) shows another defect resulting in 2 pentagons and 2 heptagons. (A colour version of this figure can be viewed online.)

Table 1
A comparison of the quantities of interests with the corresponding experiment, DFT and MD values. The last column shows the values of these properties calculated by employing the AIREBO potential. ω_1 denotes the phonon frequency at τ point for LO branch while ω_2 denotes the phonon frequency at same point for TO branch.

Properties	Experiment	DFT	MD	MD (AIREBO)
Cohesive Energy (eV)	−7.374 (graphite) [39]	7.4604, 7.906 [40],7.73 [41]	−7.401 [42]	−7.427
Lattice Constant (A^o)	2.459 [43]	2.408-2.6 [44]	2.46 [42]	2.419
Vacancy Form Energy (eV)	7.0 [45]	7.5 [46,47]		7.558
Bond Rotation Energy(eV)	5 [48]	5 [46,49]		5.294
C11 (N/m)	340 [50]	358.1 [14],342 [51,52]	348 [15], 353 [53]	331.470
C12 (N/m)		60.4 [14], 65 [51] [52],	93 [15], 58.2 [53]	112.085
$\omega_1(THz)$	46.92 [54,55]		~50.37 [56]	~53.96 [56]
$\omega_2(THz)$	47.28 [54,55]		~50.37 [56]	~53.96 [56]

potential terms and bond order are obtained using least squares fit to the force constants and energies for a range of hydrocarbons. To reduce the number of parameters, dependence in the pair potential terms were identified by constraining the sum of equations (3) and (4) to the bond energy of diamond at r_{ij} equal to its corresponding bond distance. Using the sum of equations (3) and (4), values of B_{CC3} and β_{CC3} were obtained in terms of the rest of the pair potential parameters. In the second stage, discrete value of fitted bond order term is used to obtain its corresponding functional parameters by fitting over the database of vacancy formation energies and bond rotation energies.

In the present work, we introduced variability in the REBO parameters, using the sum constraint as mentioned in the previous paragraph. By introducing variability in independent parameters, we measured the values of dependent parameters, B_{CC3} and β_{CC3}, by setting the sum of equations (3) and (4) to the bond energy of diamond (E_{CC}) at r_{ij} equal to the single C–C bond distance, r_e. Using the original fitted parameter values, the effect of single C–C bond order is measured by a constant k. Hence, sum of equations (3) and (4) is modified in the following way

$$B_{CC3}\exp(-\beta_{CC3}r_e) = E_{CC} - \left[V_{repulsion} + \sum_{n=1,2} B_{CCn}\exp(-\beta_{CCn}r_e)\right] - k, \quad (5)$$

where value of k is determined using original fittings of the parameters. For each set of the dependent and independent parameters, corresponding values of the bond order terms were obtained using equation (2). Further, values for the bond order corresponding to double, conjugated double and triple bonds are obtained by setting the derivative of equation (2) to zero at corresponding equilibrium distances. The obtained bond order terms for single, double, conjugated double and triple bonds exhibited very low variation, of the order of 10^{-3}. With such a low bond order variability, only parameters corresponding to the pair potential part are considered for uncertainty quantification studies.

2.2.2. LJ parameters and torsional term

Since fittings for LJ parameters and torsional term were done independently from the REBO parameters in Ref. [10], UQ study in the present work also considers their relations with each other as independent. Further, the three parameters for LJ and torsional term are also fitted independently of each other [10].

We will denote the parameters by σ_{CC}, ε_{CC}, ε^{T}_{CCCC}, β_{CC1}, β_{CC2}, β_{CC3}, B_{CC1}, B_{CC2}, B_{CC3}, A, Q_{CC}, α_{CC}, as detailed in Ref. [10].

2.3. Design of the UQ study

The goal is to find the posterior distribution of IP parameters, θ, which involves assessing the dependence of θ on the experimental/DFT observations, Y_{obs}. This dependence is assessed through Bayes theorem which in the current context can be written as follows

$$p(\theta|Y_{obs}) \propto p(Y_{obs}|\theta)p(\theta), \tag{6}$$

where $p(\theta|Y_{obs})$ is the posterior probability distribution of the IP parameters θ, given the experimental/DFT observations, Y_{obs}. For a particular realization of the IP parameter θ, $p(Y_{obs}|\theta)$ denotes the likelihood of observing Y_{obs} which is approximated by corresponding MD prediction. The prior, $p(\theta)$, is chosen to be a non-informative uniform prior for each IP parameter.

To obtain the likelihood, $p(Y_{obs}|\theta)$, we start by defining Y_{obs} as a realization of the true value of the QOI, Y_{true}. The discrepancy between true and observed value is denoted by measurement noise, ε_{MN} as shown in the following relation

$$Y_{obs} = Y_{true} + \varepsilon_{MN}. \tag{7}$$

Similarly, $Y_{MD}(\theta)$, the MD prediction corresponding to a parameter set θ is related to Y_{true} through the following relation

$$Y_{MD}(\theta) = Y_{true} + \varepsilon_{MD}. \tag{8}$$

The discrepancy between MD predictions and true values, denoted by ε_{MD}, can be a result of difference in initial atomic velocities, limitations on system size and simulation time, autocorrelation lengths, etc. By approximating experimental observation Y_{obs} through MD prediction $Y_{MD}(\theta)$, we assume a single noise term for both measurement as well as MD noise. It is assumed that the overall noise, ε_{Noise}, is the sum of ε_{MD} and ε_{MN} and distributed normally, i.e. $\varepsilon_{Noise} \sim N(0, \sigma^2_{Noise})$. The standard deviation, σ_{Noise}, of this distribution is treated as another parameter whose posterior probability needs to be determined. The prior of σ_{Noise} is assumed to be half normal.

Since the noise model is gaussian, the likelihood becomes

$$p\left(Y_{obs}\middle|\theta, \sigma^2_{Noise}\right) \propto \exp\left(\frac{-1}{\sigma^2_{Noise}}\left[Y_{obs} - Y_{MD}(\theta)\right]^2\right). \tag{9}$$

To evaluate the likelihood as above requires full MD simulations, which can be computationally expensive. To alleviate this computational burden, we employed efficient surrogate models based on Gaussian Process methodology which will be used to approximate the MD predictions.

Gaussian Processes (GP) [59–61] are a special class of surrogate models which are trained using input-output pairs. In the present study, pairs of IP parameters and corresponding MD predictions are used to train GP models. The MD prediction $Y_{MD}(\theta)$ can be related to the mean GP prediction, $\mu_{GPM}(\theta)$, through the following relation

$$Y_{MD}(\theta) = \mu_{GPM}(\theta) + \sigma^2_{GPM}(\theta), \tag{10}$$

where $\sigma^2_{GPM}(\theta)$ is the variance or the uncertainty about the mean prediction of GP models.

Using the preceding equations, the relationship between the GP prediction, $\mu_{GPM}(\theta)$, and Y_{obs} can be written as

$$Y_{obs} = \mu_{GPM}(\theta) + \sigma^2_{GPM}(\theta) + \varepsilon_{Noise}. \tag{11}$$

A critical part of a GP model is the covariance function which dictates correlations between GP predictions for two distinct input points. The choice of covariance function can affect the quality of the GP prediction. We tested a number of covariance functions and the best predictor is used for further analysis. Performance of each GP model is assessed using the leave-one out error which is calculated by training the model using the entire training set except one point. GP prediction on the left-out point is compared to the corresponding MD prediction at that point and an error is recorded. This process is repeated for all the remaining training points which gives a mean absolute error corresponding to that GP model structure. The goal is to select the GP model which minimizes this mean error. Further, the MD prediction is compared with the GP model prediction and R-Squared value is computed from a straight-line fitting between these two predictions. R-Squared value along with normalized root mean square error is used to assess the performance of each surrogate model.

The approximation of MD prediction through GP models leads to the following likelihood function

$$p\left(Y_{obs}\middle|\theta, \sigma^2_{Noise}, \sigma^2_{GPM}\right) \propto \exp\left(-\left[Y_{obs} - \mu_{GPM}(\theta)\right]\Sigma^{-1}\left[Y_{obs} - \mu_{GPM}(\theta)\right]^T\right), \tag{12}$$

where Σ is the diagonal covariance matrix with each element given by the sum of the variance of the GP prediction, σ^2_{GPM}, and measurement noise, σ^2_{Noise}. In the present work, likelihood maximization translates into minimization of the maximum variation between experimental value and MD prediction (approximated through GP prediction). Given the high-dimensional nature of the likelihood function, the posterior distribution of the IP parameters, as per equation (6), is estimated using a Markov Chain Monte Carlo (MCMC) scheme [62]. The detailed distributions for the IP parameters and the corresponding statistics are presented in the results section.

3. Results and discussion

In order to assess the sensitivity of QOI to IP parameters, we randomly perturbed the parameters and performed MD simulations on the perturbed parameter set. Instead of using random sampling, more efficient sampling based on Quasi Monte-

Carlo(QMC) procedures is employed to cover the input space more effectively. Pseudo random numbers based on the low discrepancy Sobol sequence [63,64] are generated and used to perturb the IP parameters, θ, through the following relations

$$\theta_{min} = \theta(1-\delta); \quad \theta_{max} = \theta(1+\delta) \quad \delta \in \{0.01\%, 0.1\%, 0.3\%, 0.5\%, 1\%\}, \tag{13}$$

$$\theta_i = \theta_{min} + (\theta_{max} - \theta_{min})SP_i \quad i \in \{1, 2, \ldots N\}, \tag{14}$$

where δ is the percentage variation with which original fitted values are perturbed. For a corresponding value of δ, the range is defined by the difference of maximum and minimum value of perturbed IP parameters. Considering the i-th Sobol point, SP_i, and the range of perturbation, an i-th perturbed IP parameter vector, θ_i, is obtained using equation (14).

For different values of δ, corresponding sets of 500 independent parameter vectors were obtained using the above relations. Each parameter vector is of dimensionality 10, equal to the number of IP parameters. For each vector, independent MD simulations are performed to obtain the respective QOI. MD simulations are performed using LAMMPS [36]. We started with a very small variation of 0.01% and then slowly increased it to 0.1%, 0.3%, 0.5%, 1%. The results for these variations are shown in Fig. 2 and the main statistics are documented in Table 2.

It can be observed from the box plots and Table 2, that output QOIs are extremely sensitive, with observations off by 400% from the reference MD values (Bond rotation energy). Even the signature properties for a material structure, cohesive energy, lattice constants and elastic constants, showed high sensitivity to the small changes in the IP parameters. Higher-order properties like bond rotation energy showed a number of outliers on a small change of 0.5% with an unphysical mean value of −18.16 eV. Further, variance in the properties like elastic constants and bond rotation energy is very high ($>10^3$), which shows the fragile nature of the AIREBO potential.

Table 2
Statistics for the QOIs at uncertainty level of 0.5%. Mean of the properties, shown in first column, stayed closer to MD values except the bond rotation energy. Further, variance, shown in the last column, is very high for the higher-order properties.

Property	Mean	Minimum	Maximum	Range	Variance
Cohesive energy	−7.48	−9.62	−6.13	3.5	10.76
Lattice constant	2.42	2.24	2.55	0.31	0.005
C_{11}	331.21	241.77	430.66	188.89	1939.01
C_{12}	117.93	95.63	181.69	86.06	237.88
Vacancy energy	7.63	5.26	10.37	5.11	1.18
Bond rotation energy	−18.16	−384.41	5.34	389.76	3505.07
ω_1	936.92	160.54	5459.36	5298.83	622219.3
ω_2	178.67	1.26	700.46	699.20	26057

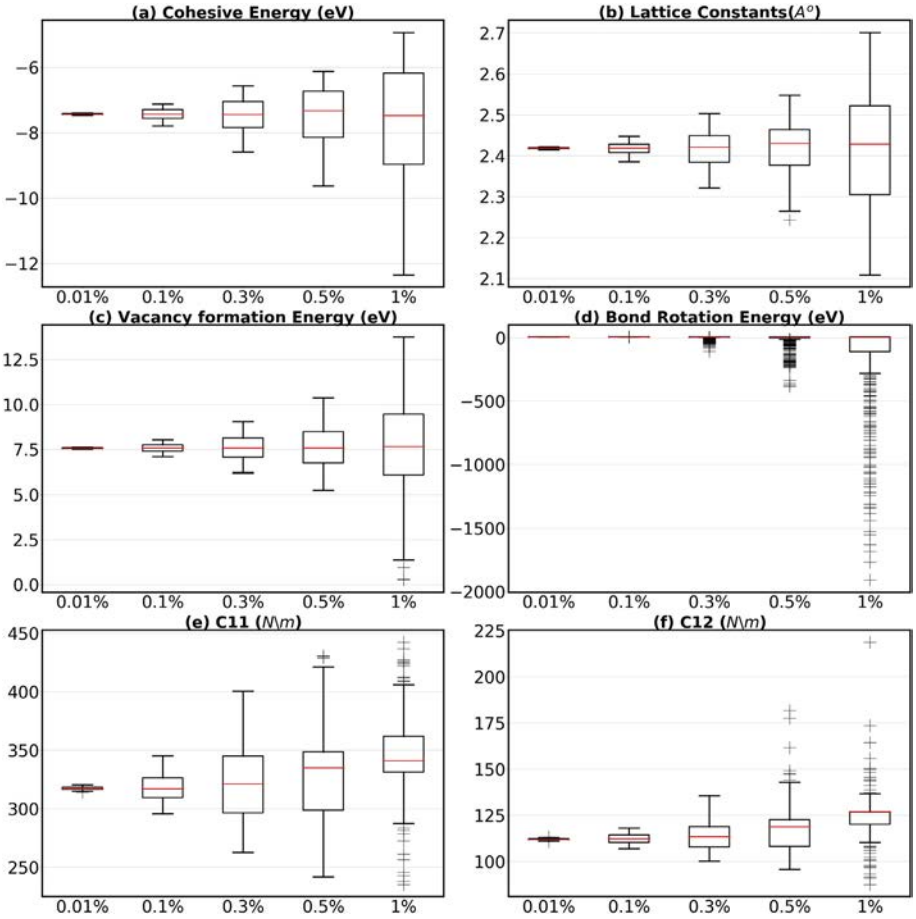

Fig. 2. Boxplots showing the variation of the range of properties for various values of uncertainties. Small variations in the parameters (0.3%) produced huge variation in basic property like cohesive energy. Further increasing uncertainty to 1% led to a number of outliers in defect formation energies. Elastic constants shown (e) and (f) also indicate presence of a number of outliers at δ equal to 1%. (A colour version of this figure can be viewed online.)

3.1. Correlation between inputs and outputs

Examining the scatter plots for each QOI with respect to the input parameters, it can be seen that most of the parameters have no significant effect on the final properties of interest except α_{CC}. Fig. 3 shows the scatter plots of various QOIs with respect to α_{CC}. While cohesive energy and elastic constants show a nearly linear relationship, the bond rotation energy showed non-linear behavior.

3.2. Gaussian processes model training

For training the GP models, we considered MD predictions from the last section, corresponding to $\delta = 0.5\%$. Out of 500 MD simulations, only 200 simulations were used to train the models. Training of each GP model is carried out using a python package, GPy [65], where hyperparameters for each model are obtained by maximum likelihood estimation.

To validate the GP models, we used the leave-one out (LOO) criteria and corresponding plots are appended in the supporting information, SI 4. For all the QOI, the plots are linear showing GP predictions are aligned with MD results. To validate further, R-squared value of the line fitting the GP prediction and MD data is presented in Table 3. It is observed that R-squared value for GP models is more than 0.9. Additional performance metrics used for the GP model validation is normalized root mean square error. From Table 3, it is observed that highest normalized mean square error is of the order of 10^{-2}. The above validation metrics suggest that the GP models have sufficient predictive accuracy.

Using GP models, predictions of each QOI are made for each perturbed IP, θ_i, and corresponding statistics are documented in Table 4. Comparing the results in Table 4 to the ones in Table 2, its easily evident that statistics for each QOIs are very close to each other. Thus, from the validation metrics provided in the last section along with the comparable statistics to full MD runs, justifies our use of GP models. GP models were trained using a subset of MD simulations data, which significantly reduced the computational burden of UQ studies for MD.

Table 3
Validation metrics for various GP models. The first column shows the type of the kernel used for the corresponding QOI followed by normalized mean square error denoted as MSE.

Property	Kernel	Normalized MSE	R-Squared
Cohesive energy	RBF	1.69×10^{-3}	0.99
Lattice constant	RBF	3.74×10^{-3}	0.99
C_{11}	RBF	0.032	0.95
C_{12}	RBF	0.038	0.92
Vacancy energy	RBF	0.0047	0.99
Bond rotation energy	RBF	0.0063	0.99
ω_1	RBF*RBF	10^{-8}	0.99
ω_2	RBF*RBF	10^{-8}	0.99

Another check for the GP models was performed by considering a sample of 10,000 uniformly distributed IP parameters obtained through random sampling within δ (set to 0.5%) of the fitted values. For this test sample, predictions for each QOI are made using corresponding GP models and statistics for each are documented in supporting information SI 5. Comparing the range of the values in QOI obtained through QMC and random sampling reveals that there are certain points in Sobol space which are causing the highest variation resulting in extremely high values for the final values of the QOI. Of all the QOI, GP predictions for the bond rotation energy showed the highest expected value for variance, which can be reduced by considering more MD runs during training of its corresponding GP model.

Assessment of the probabilities that GP prediction for a QOI lies within a certain range of corresponding DFT values were performed. Our results indicate that probability values through GP models match the ones computed from 500 MD simulations. The results are appended in supporting information, SI 6.

3.3. Markov Chain Monte Carlo

To approximate the posterior distributions of the IP parameters, a MCMC algorithm is implemented using the PyMC3 library [66].

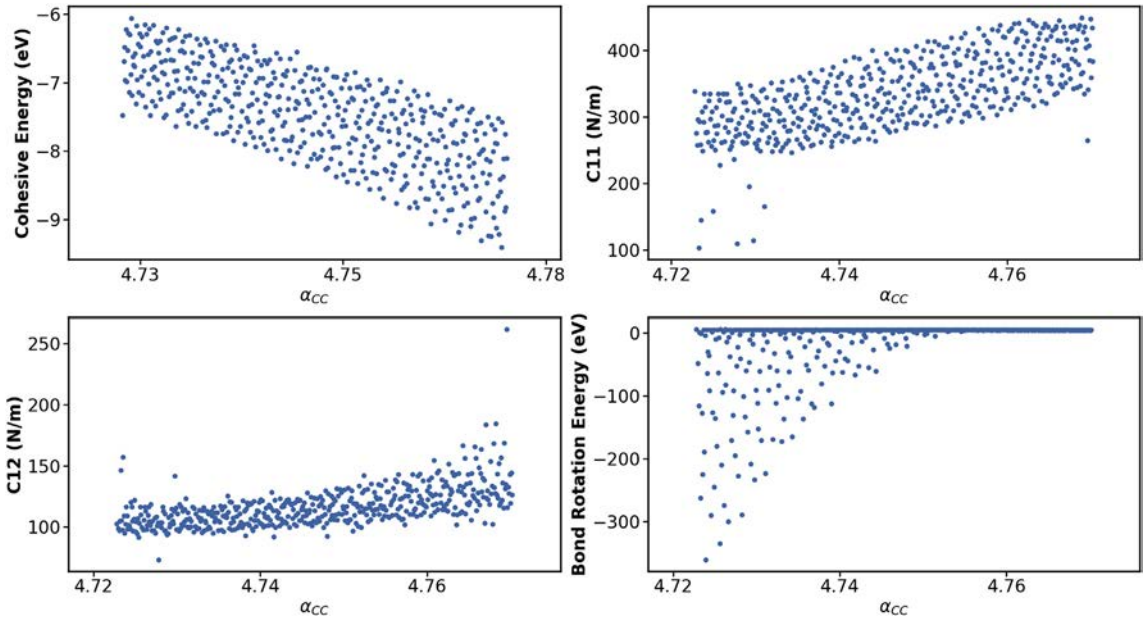

Fig. 3. Scatter of QOIs with respect to α_{CC}. The variation is approximately linear for cohesive energy and C_{11} while non-linear for C_{12}. A trend can be seen for the cohesive energy and elastic constants while no trend is visible for the bond rotation energy. (A colour version of this figure can be viewed online.)

Table 4
Posterior distributions of the corresponding QOIs. The above QOIs are computed on the 500 points from the previous section. For notational brevity, $z(\theta)$ denotes the $\mu_{GPM}(\theta)$ in this table. The last column denotes the variance in expected value of GP prediction for a QOI.

Property	E[$z(\theta)$]	min($z(\theta)$)	max($z(\theta)$)	Range	var($z(\theta)$)
Cohesive energy	−7.488	−9.614	−5.952	3.66	0.731
Lattice constant	2.418	2.243	2.581	0.34	0.005
C_{11}	337.25	229.33	442.93	213.61	2156.88
C_{12}	118.39	93.66	160.81	67.15	184.43
Vacancy energy	7.63	5.552	10.348	4.80	1.18
Bond rotation energy	−18.03	−367.6	9.07	376.67	3468.13
ω_1	936.92	160.54	5459.36	5298.83	622219.3
ω_2	178.67	1.26	700.46	699.20	26057

Using the noise models, likelihood and priors as described in the earlier section, four separate MCMC chains were run with sample length of 80,000 each. To assess if the chain has reached stationarity, Gwekes indices procedure was applied which confirms that all the sampled points lies between ±1 of their corresponding standard deviation. Fig. 4 shows auto-correlation plots for each parameter, which alongwith traceplots further confirms stability of the MCMC chain.

Considering the burnout of size 15000, a thinning heuristic of selecting every 10^{th} point is applied on the remaining 65000 samples. From the thinned MCMC chain samples, the posterior probability distribution for each parameter is obtained and corresponding plots are shown in Fig. 5, with corresponding statistics as documented in Table 5. The dashed line in Fig. 5 denotes the original AIREBO fitted parameter values.

From Fig. 5 and Table 5, it is clear that REBO parameters i.e. B_{CC1}, B_{CC2} and Q_{CC} are the most critical parameters with huge deviation of their original fitted values from the corresponding MCMC sample mean. Parameters like β_{CC2} and β_{CC3} also have mean different than the fitted values. Given that we considered very small uncertainty of 0.5% in the training set or in our prior, the mean of the parameters differs by 0.5%. Higher uncertainty in the training sets might lead to higher variations in the mean values. With posterior distribution same as prior distribution, LJ parameter (ε_{CC}) exhibit no significant influence on the sensitivity of the QOI. All the parameter posterior distributions have very low variance denoting the high confidence in the predicted mean values of these parameters.

A posterior predictive check is performed using a test sample of 1000 parameter sets, obtained from the sampled posterior distributions. For the test set, corresponding GP models were used to obtain predictions for each QOI. Fig. 6 shows the boxplots of the GP predictions for the test sample with corresponding statistics as shown in Table 6. An estimate of the mean value of σ^2_{Noise} is also documented in Table 6. In the sampling scheme, we approximated the weightage of phonon frequencies to be equal to 0.1 which led to stable MCMC chains. For fitting purposes, it means giving relatively higher weightage to cohesive energy and lattice constant than phonon frequencies. With this sampling choice, parameters returned with very high GP variance for phonon frequencies. As a sanity check, we performed MD simulations to compute phonon frequencies using a subset of posterior distribution. The predicted values of phonon frequencies exhibited the similar trend as shown in Fig. 6.

It can be observed from Fig. 6 and Table 6, that the predicted properties are very close to DFT values except C_{12}. Scatter in the

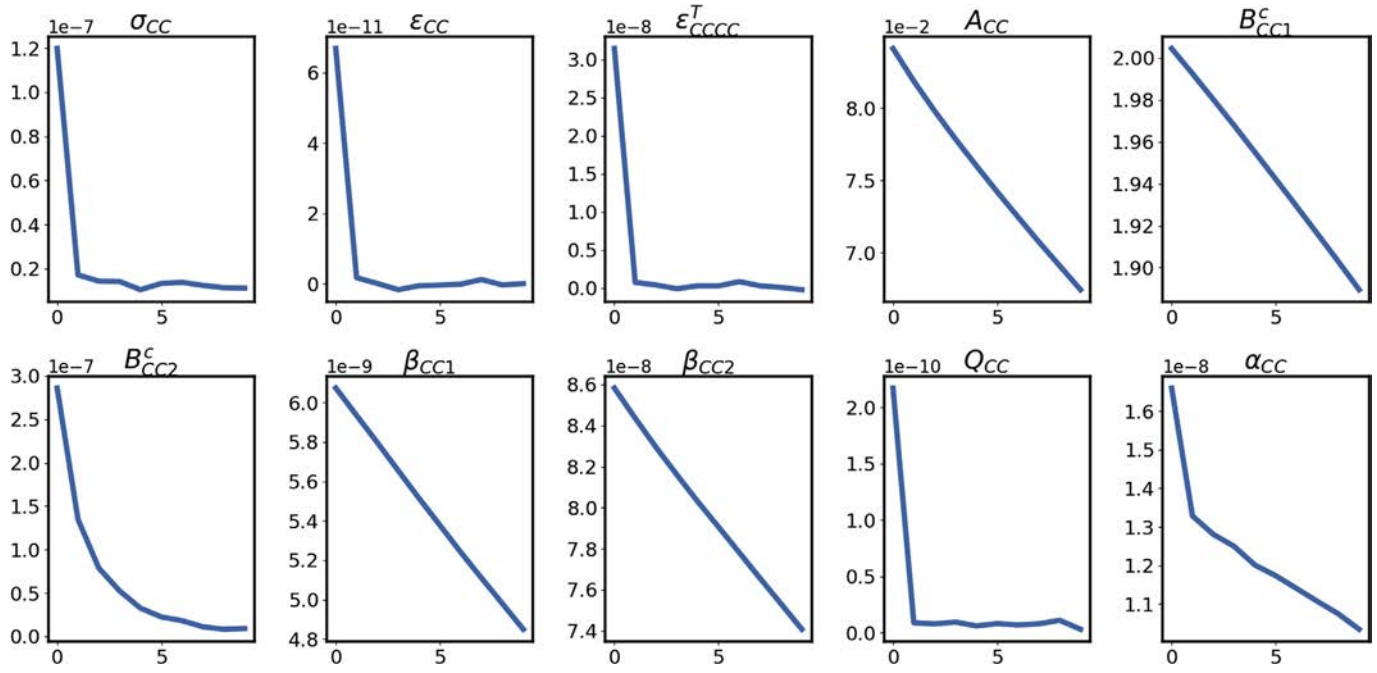

Fig. 4. Auto-covariance function for each parameter with respect to the lag length. Horizontal axis in each plot denotes the lag length used in determining autocorrelation of the posterior distribution. (A colour version of this figure can be viewed online.)

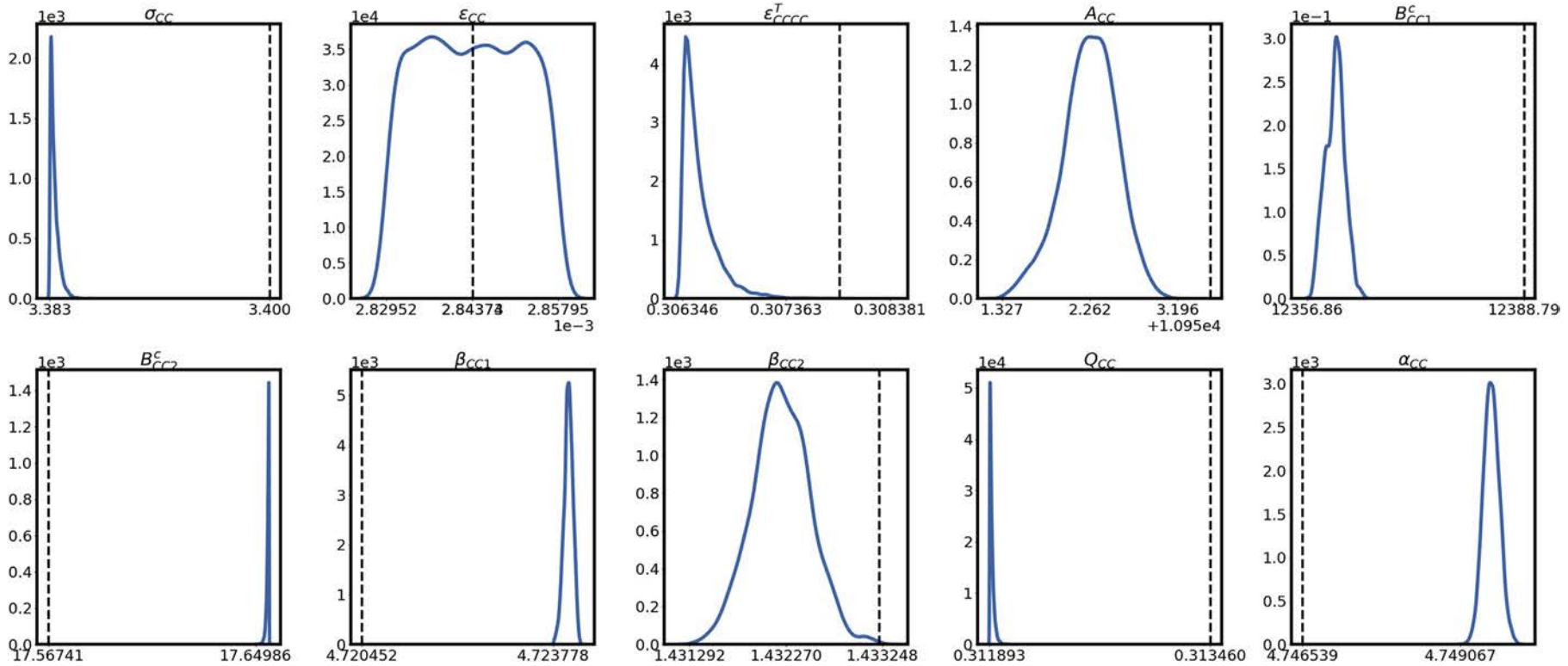

Fig. 5. Distribution plots for each parameter after applying thinning algorithms to MCMC trace. For each parameter, its corresponding reference fitted value is shown by the dashed black line. (A colour version of this figure can be viewed online.)

Table 5
Statistics for the posterior probability distribution in the IP parameters.The first row of this table denotes the reference IP parameter values before applying any perturbation. Second row details the mean values of the posterior distribution and percentage change of the mean values from reference values are detailed in the subsequent row. Following two rows details the percentage change in minimum and maximum values from the reference values.

Metric	σ_{CC}	ε_{CC}	ε^{T}_{CC}	A_{CC}	B_{CC1}
Original	3.4	0.0028	0.307885	10953.54	12388.79
Mean	3.38	2.84363×10^{-3}	0.306517	10952.26	12360.98
Mean % change	0.49	0.00357	0.44	0.012	0.23
Min % change	0.49	0.5	0.5	0.02	0.26
Max % change	0.41	0.5	0.16	0.0032	0.189
Variance	10^{-7}	10^{-11}	10^{-8}	0.084	2.004
Metric	B_{CC2}	β_{CC1}	β_{CC2}	Q_{CC}	α_{CC}
Original	17.567	4.72045	1.433213	0.313460	4.746539
Mean	17.66	4.724	1.4322	0.31191	4.749
Mean % change	0.497	0.076	0.069	0.495	0.0637
Min % change	0.469	0.07	0.134	0.5	0.053
Max % change	0.5	0.081	0.0024	0.45	0.073
Variance	10^{-7}	10^{-9}	10^{-8}	10^{-10}	10^{-8}

properties are more reasonable and analogous to the distribution due to the measurement noise. Compared to the sensitivity results provided in the previous section, elastic constants and bond rotation energy are within 3 standard deviations of their corresponding mean values. Expected value for the variance in GP predictions for elastic constants and bond rotation energy is high, which can be decreased by considering more MD runs for these QOI during GP training. Of the properties considered here, only C_{12} has very high standard deviation for measurement noise. A possible reason for this is the discrepancy between corresponding MD and DFT values from literature. Our GP training dataset corresponds to MD value of 112 N/m while MCMC model tries to maximize likelihood with respect to DFT value of 65 N/m. This discrepancy in GP training and DFT observation is captured through measurement noise, refer Table 6.

3.4. Thermal conductivity

Analysis of the thermal properties based on the obtained posterior probability of IP parameters is performed in this section. We

Table 6
Statistics for various quantities of interest as compared to the corresponding DFT values. Above predictions are obtained for a random sample of 1000 parameters obtained from corresponding posterior distributions. Also shown are the predictions from posterior predictive distributions (PPC) with expected standard deviation of the measurement noise. For notation brevity, $z(\theta)$ is used to represent $\mu_{GPM}(\theta)$.

Property	DFT	$E[z(\theta)]$	$\mathrm{var}(z(\theta))$	$E[\sigma^2_{GPM}(\theta)]$	$E[\sigma^2_{Noise}]$
Cohesive energy	−7.73	−7.61	10^{-5}	10^{-5}	10^{-3}
Lattice constant	2.46	2.42	10^{-7}	10^{-6}	10^{-3}
C_{11}	342	321.07	10^{-2}	2.48	0.43
C_{12}	65	114.13	10^{-2}	0.45	4.38
Vacancy energy	7.5	7.75	10^{-3}	10^{-4}	10^{-3}
Bond rotation energy	5	5.49	10^{-4}	10^{-1}	0.39
ω_1		48.04	10^{-1}	10^{5}	
ω_1		48.23	10^{-2}	10^{4}	

computed thermal conductivity of a graphene sheet with dimensions of 100×10 A^o, using non-equilibrium MD method. Similar methodology is adopted in Ref. [67] for thermal conductivity predictions. Using the AIREBO potential, thermal conductivity was computed to be 443 W/mK, which is significantly lower than the experimental and DFT values. Thermal conductivity computed using optimized Tersoff potential [68] for the same sheet is 482.91 W/mK. It has been established in previous studies that AIREBO is well suited for C–C bond breaking systems and performs poorly for thermal properties [56,67,69]. In order to improve the prediction of thermal properties through AIREBO, it is necessary to address limitations related to its functional form, which is not the focus of the present study. To have consistent UQ analysis for all the output properties, we have performed analysis of thermal conductivity relative to the AIREBO value.

To assess the sensitivity of thermal conductivity with respect to changes in IP parameters, 500 independent MD simulations were performed at δ equal to 0.5% and corresponding results are shown in Fig. 7 (a). It can be easily seen that values of thermal conductivity are extremely sensitive to small changes in IP parameters, with values varying between 349 W/mk and 600 W/mk. Using this data, efficient GP model, with MSE of the order of 10^{-5} was trained and used for UQ analysis.

Fig. 7 (b) shows the GP model's predictions for thermal conductivity at the obtained posterior distribution of the IP

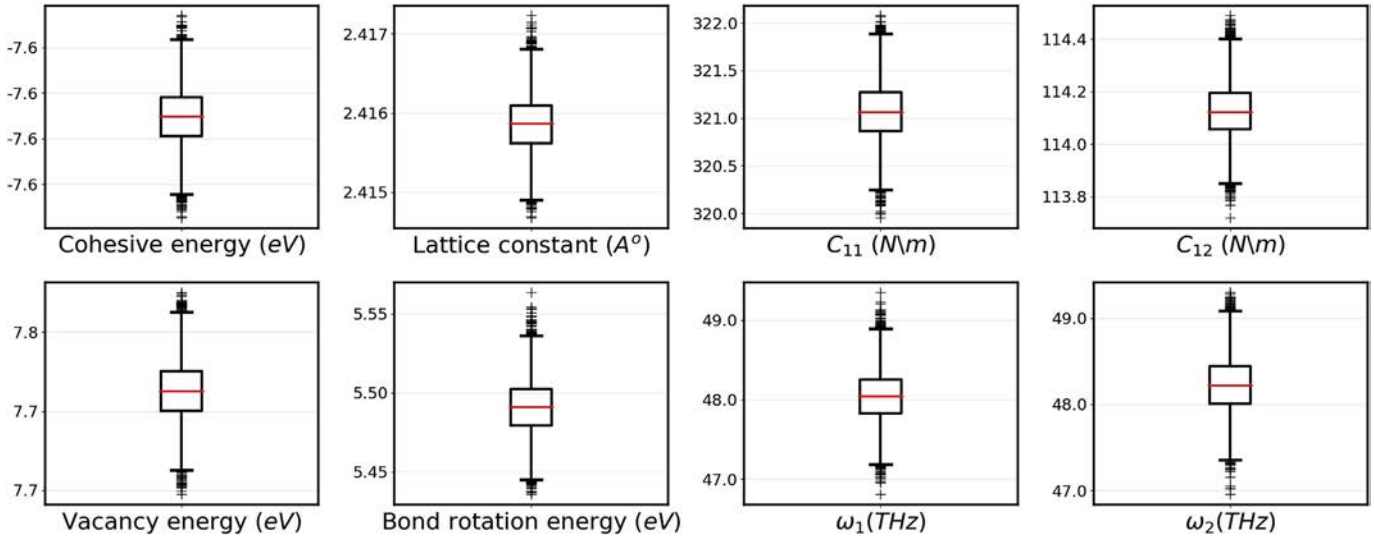

Fig. 6. Boxplots of various QOIs corresponding to a test sample of 1000 parameters from posterior distributions. Comparing to sensitivity analysis results in Fig. 2, the properties are scattered relatively less. (A colour version of this figure can be viewed online.)

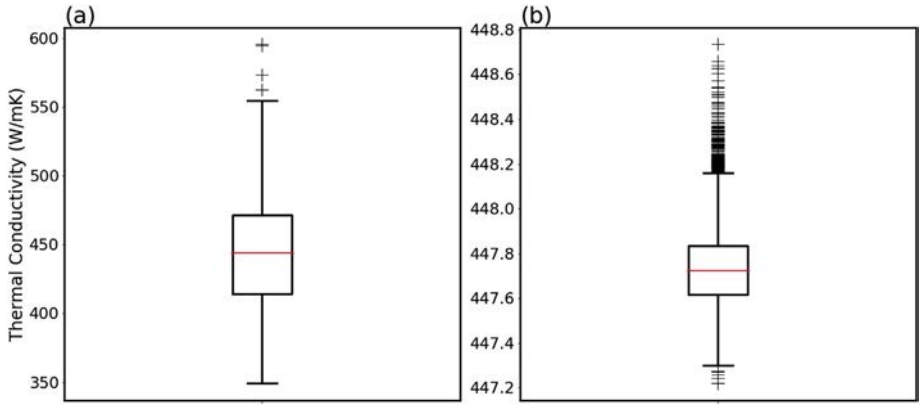

Fig. 7. Boxplots showing the variation of thermal conductivity for a.) MD simulations at δ equal to 0.5% and, b.) GP model's prediction on the posterior distribution of IP parameters. (A colour version of this figure can be viewed online.)

parameters. As compared to the MD results using Sobol points, the posterior predictions of thermal conductivity are closer to the AIREBO/Tersoff value and are exhibiting very low sensitivity towards change in the IP parameters.

4. Conclusions

In this study, we investigated the sensitivity of MD predictions of graphene properties, using the AIREBO potential, with respect to the corresponding IP parameters. Our work showed that quantities of interest (QOI) such as cohesive energy, lattice constants, elastic constants and defect energies are highly sensitive to small changes in the Interatomic Potential (IP) parameters. A small change of 0.5% resulted in an order of magnitude change (up to 66%) in characteristic properties such as cohesive energy, lattice constant and elastic constants. Assuming a gaussian likelihood model, we obtained a new robust IP parameter set for the AIREBO potential which addresses the sensitivity issues in its original parameters. Most of the parameter distributions in this new set are far from their original fitted values. In contrast, two-body contributions of the IP modeled through the Lennard Jones potential parameter, ϵ_{CC} were found to have low impact on sensitivity of QOI and the mean of corresponding two-body parameters remained closer to their original fitted value. On the other hand, the REBO parameters were found to be very sensitive, indicating that future studies should focus more on these parameters.

Since our analysis considered the latest DFT predictions of graphene from the literature, we believe our new IP parameter set is better suited to modeling graphene than the original AIREBO potential parameter setting. We found that modeling the uncertainty in the IP parameters using posterior probability distributions and propagating to the QOI can increase reliability in MD predictions. The proposed framework is a computationally efficient tool for investigating the suitability of IP parameters for modeling conditions which are outside their original fitting dataset, as exhibited through thermal conductivity predictions. In addition, the proposed framework can also be applied to assess the probability distribution of the QOI not considered during the original fitting process.

Acknowledgements

Support from Natural Sciences and Engineering Research Council of Canada, Hart Professorship, University of Toronto is appreciated. We are grateful to valuable resources provided by Compute Canada to perform MD simulations.

Appendix A. Supplementary data

Supplementary data to this article can be found online at https://doi.org/10.1016/j.carbon.2018.10.020.

References

[1] P.N. Patrone, A. Dienstfrey, A.R. Browning, S. Tucker, S. Christensen, Uncertainty quantification in molecular dynamics studies of the glass transition temperature, Polymer 87 (2016) 246–259.
[2] S.T. Reeve, A. Strachan, Error correction in multi-fidelity molecular dynamics simulations using functional uncertainty quantification, J. Comput. Phys. 334 (2017) 207–220.
[3] P.N. Patrone, T.W. Rosch, F.R. Phelan Jr., Bayesian calibration of coarse-grained forces: efficiently addressing transferability, J. Chem. Phys. 144 (15) (2016) 154101.
[4] I.H. Son, J.H. Park, S. Park, K. Park, S. Han, J. Shin, et al., Graphene balls for lithium rechargeable batteries with fast charging and high volumetric energy densities, Nat. Commun. 8 (1) (2017) 1561.
[5] M.J. Allen, V.C. Tung, R.B. Kaner, Honeycomb carbon: a review of graphene, Chem. Rev. 110 (1) (2009) 132–145.
[6] M. Inagaki, Y. Kim, M. Endo, Graphene: preparation and structural perfection, J. Mater. Chem. 21 (10) (2011) 3280–3294.
[7] Y. Sun, Q. Wu, G. Shi, Graphene based new energy materials, Energy Environ. Sci. 4 (4) (2011) 1113–1132.
[8] W. Choi, I. Lahiri, R. Seelaboyina, Y.S. Kang, Synthesis of graphene and its applications: a review, Crit. Rev. Solid State Mater. Sci. 35 (1) (2010) 52–71.
[9] Y. Hancock, The 2010 nobel prize in physicsground-breaking experiments on graphene, J. Phys. Appl. Phys. 44 (47) (2011) 473001.
[10] S.J. Stuart, A.B. Tutein, J.A. Harrison, A reactive potential for hydrocarbons with intermolecular interactions, J. Chem. Phys. 112 (14) (2000) 6472–6486.
[11] G. Jo, A.M. Haque, S. Kim, H. Jeong, H. Chung, Physical properties variation of graphene and multi wall carbon nanotubes by planetary ball mill and heat treatment, in: IOP Conference Series: Materials Science and Engineering, vol. 88, IOP Publishing, 2015, p. 012054.
[12] V. Singh, D. Joung, L. Zhai, S. Das, S.I. Khondaker, S. Seal, Graphene based materials: past, present and future, Prog. Mater. Sci. 56 (8) (2011) 1178–1271.
[13] H. Sahlaoui, M. Guedri, H. Sidhom, Effect of uncertainty parameters on graphene sheets youngs modulus prediction, J. Mech. Sci. Technol. 27 (9) (2013) 2769–2774.
[14] X. Wei, B. Fragneaud, C.A. Marianetti, J.W. Kysar, Nonlinear elastic behavior of graphene: Ab initio calculations to continuum description, Phys. Rev. B 80 (20) (2009) 205407.
[15] K. Fair, M. Arnold, M. Ford, Determination of the elastic properties of graphene by indentation and the validity of classical models of indentation, J. Phys. Condens. Matter 26 (1) (2013), 015307.
[16] A.C. Neto, F. Guinea, N.M. Peres, K.S. Novoselov, A.K. Geim, The electronic properties of graphene, Rev. Mod. Phys. 81 (1) (2009) 109.
[17] H.N. Najm, Uncertainty quantification and polynomial chaos techniques in computational fluid dynamics, Annu. Rev. Fluid Mech. 41 (2009) 35–52.
[18] A. Chernatynskiy, S.R. Phillpot, R. LeSar, Uncertainty quantification in multiscale simulation of materials: a prospective, Annu. Rev. Mater. Res. 43 (2013) 157–182.
[19] C.A. Becker, F. Tavazza, L.E. Levine, Implications of the choice of interatomic potential on calculated planar faults and surface properties in nickel, Phil. Mag. 91 (27) (2011) 3578–3597.
[20] C.A. Becker, F. Tavazza, Z.T. Trautt, R.A.B. de Macedo, Considerations for choosing and using force fields and interatomic potentials in materials science

and engineering, Curr. Opin. Solid State Mater. Sci. 17 (6) (2013) 277–283.
[21] C. Wong, H. Rabitz, Sensitivity analysis and principal component analysis in free energy calculations, J. Phys. Chem. 95 (24) (1991) 9628–9630.
[22] T. Kristóf, J. Liszi, Sensitivity analysis of some thermodynamic properties of 2-centres Lennard-Jones liquids, Z. Phys. Chem. 190 (2) (1995) 289–297.
[23] T. Kristóf, J. Liszi, Sensitivity analysis of the vapour-liquid phase equilibria of a model of liquid carbon disulphide, Z. Phys. Chem. 194 (2) (1996) 263–272.
[24] S.-B. Zhu, C.F. Wong, Sensitivity analysis of water thermodynamics, J. Chem. Phys. 98 (11) (1993) 8892–8899.
[25] F. Hanke, Sensitivity analysis and uncertainty calculation for dispersion corrected density functional theory, J. Comput. Chem. 32 (7) (2011) 1424–1430.
[26] S.-B. Zhu, C.F. Wong, Sensitivity analysis of a polarizable water model, J. Phys. Chem. 98 (17) (1994) 4695–4701.
[27] S.L. Frederiksen, K.W. Jacobsen, K.S. Brown, J.P. Sethna, Bayesian ensemble approach to error estimation of interatomic potentials, Phys. Rev. Lett. 93 (16) (2004) 165501.
[28] D. Kim, F. Rizzi, K.W. Cheng, J. Han, F. Bisetti, O.M. Knio, Uncertainty quantification of ion chemistry in lean and stoichiometric homogenous mixtures of methane, oxygen, and argon, Combust. Flame 162 (7) (2015) 2904–2915.
[29] M. Salloum, K. Sargsyan, R. Jones, B. Debusschere, H.N. Najm, H. Adalsteinsson, A stochastic multiscale coupling scheme to account for sampling noise in atomistic-to-continuum simulations, Multiscale Model. Simul. 10 (2) (2012) 550–584.
[30] F. Rizzi, H.N. Najm, B.J. Debusschere, K. Sargsyan, M. Salloum, H. Adalsteinsson, et al., Uncertainty quantification in md simulations. part ii: Bayesian inference of force-field parameters, Multiscale Model. Simul. 10 (4) (2012) 1460–1492.
[31] F. Cailliez, P. Pernot, Statistical approaches to forcefield calibration and prediction uncertainty in molecular simulation, J. Chem. Phys. 134 (5) (2011), 054124.
[32] F. Rizzi, M. Salloum, Y. Marzouk, R.-G. Xu, M. Falk, T. Weihs, et al., Bayesian inference of atomic diffusivity in a binary ni/al system based on molecular dynamics, Multiscale Model. Simul. 9 (1) (2011) 486–512.
[33] F. Cailliez, A. Bourasseau, P. Pernot, Calibration of forcefields for molecular simulation: sequential design of computer experiments for building cost-efficient kriging metamodels, J. Comput. Chem. 35 (2) (2014) 130–149.
[34] F. Rizzi, H.N. Najm, B.J. Debusschere, K. Sargsyan, M. Salloum, H. Adalsteinsson, et al., Uncertainty quantification in md simulations. part i: forward propagation, Multiscale Model. Simul. 10 (4) (2012) 1428–1459.
[35] P. Pernot, F. Cailliez, A critical review of statistical calibration/prediction models handling data inconsistency and model inadequacy, AIChE J. 63 (10) (2017) 4642–4665.
[36] S. Plimpton, Fast parallel algorithms for short-range molecular dynamics, J. Comput. Phys. 117 (1) (1995) 1–19.
[37] A. Stukowski, Visualization and analysis of atomistic simulation data with ovito–the open visualization tool, Model. Simulat. Mater. Sci. Eng. 18 (1) (2009), 015012.
[38] A. Fasolino, J. Los, M.I. Katsnelson, Intrinsic ripples in graphene, Nat. Mater. 6 (11) (2007) 858.
[39] L. Li, S. Reich, J. Robertson, Defect energies of graphite: density-functional calculations, Phys. Rev. B 72 (18) (2005) 184109.
[40] H. Shin, S. Kang, J. Koo, H. Lee, J. Kim, Y. Kwon, Cohesion energetics of carbon allotropes: quantum Monte Carlo study, J. Chem. Phys. 140 (11) (2014) 114702.
[41] L. Shulenburger, T.R. Mattsson, Quantum Monte Carlo applied to solids, Phys. Rev. B 88 (24) (2013) 245117.
[42] L. Lindsay, D. Broido, Optimized tersoff and brenner empirical potential parameters for lattice dynamics and phonon thermal transport in carbon nanotubes and graphene, Phys. Rev. B 81 (20) (2010) 205441.
[43] Y. Baskin, L. Meyer, Lattice constants of graphite at low temperatures, Phys. Rev. 100 (2) (1955) 544.
[44] H. Behera, G. Mukhopadhyay, Structural and electronic properties of graphene and silicene: an fp-(l) apw+ lo study, in: AIP Conference Proceedings, vol. 1313, AIP, 2010, pp. 152–155.
[45] P. Thrower, R. Mayer, Point defects and self-diffusion in graphite, Phys. Status Solidi 47 (1) (1978) 11–37.
[46] F. Banhart, J. Kotakoski, A.V. Krasheninnikov, Structural defects in graphene, ACS Nano 5 (1) (2010) 26–41.
[47] Y. Ma, P. Lehtinen, A.S. Foster, R.M. Nieminen, Magnetic properties of vacancies in graphene and single-walled carbon nanotubes, New J. Phys. 6 (1) (2004) 68.
[48] J. Kotakoski, J. Meyer, S. Kurasch, D. Santos-Cottin, U. Kaiser, A. Krasheninnikov, Stone-wales-type transformations in carbon nanostructures driven by electron irradiation, Phys. Rev. B 83 (24) (2011) 245420.
[49] J. Ma, D. Alfè, A. Michaelides, E. Wang, Stone-wales defects in graphene and other planar s p 2-bonded materials, Phys. Rev. B 80 (3) (2009), 033407.
[50] C. Lee, X. Wei, J.W. Kysar, J. Hone, Measurement of the elastic properties and intrinsic strength of monolayer graphene, Science 321 (5887) (2008) 385–388.
[51] R. Wang, S. Wang, X. Wu, X. Liang, First-principles calculations on third-order elastic constants and internal relaxation for monolayer graphene, Phys. B Condens. Matter 405 (16) (2010) 3501–3506.
[52] T. Shao, B. Wen, R. Melnik, S. Yao, Y. Kawazoe, Y. Tian, Temperature dependent elastic constants and ultimate strength of graphene and graphyne, J. Chem. Phys. 137 (19) (2012) 194901.
[53] J. Zhou, R. Huang, Internal lattice relaxation of single-layer graphene under in-plane deformation, J. Mech. Phys. Solid. 56 (4) (2008) 1609–1623.
[54] J. Maultzsch, S. Reich, C. Thomsen, H. Requardt, P. Ordejón, Phonon dispersion in graphite, Phys. Rev. Lett. 92 (7) (2004), 075501.
[55] M. Mohr, J. Maultzsch, E. Dobardžić, S. Reich, I. Milošević, M. Damnjanović, A. Bosak, M. Krisch, C. Thomsen, Phonon dispersion of graphite by inelastic x-ray scattering, Phys. Rev. B 76 (3) (2007), 035439.
[56] E.N. Koukaras, G. Kalosakas, C. Galiotis, K. Papagelis, Phonon properties of graphene derived from molecular dynamics simulations, Sci. Rep. 5 (2015) 12923.
[57] J.-W. Jiang, Parametrization of stillinger–weber potential based on valence force field model: application to single-layer mos2 and black phosphorus, Nanotechnology 26 (31) (2015) 315706.
[58] D.W. Brenner, O.A. Shenderova, J.A. Harrison, S.J. Stuart, B. Ni, S.B. Sinnott, A second-generation reactive empirical bond order (rebo) potential energy expression for hydrocarbons, J. Phys. Condens. Matter 14 (4) (2002) 783.
[59] M.C. Kennedy, A. O'Hagan, Bayesian calibration of computer models, J. Roy. Stat. Soc. B 63 (3) (2001) 425–464.
[60] A. OHagan, Bayesian analysis of computer code outputs: a tutorial, Reliab. Eng. Syst. Saf. 91 (10–11) (2006) 1290–1300.
[61] C.E. Rasmussen, Gaussian processes in machine learning, in: Advanced Lectures on Machine Learning, Springer, 2004, pp. 63–71.
[62] A.F. Smith, G.O. Roberts, Bayesian computation via the gibbs sampler and related Markov chain Monte Carlo methods, J. Roy. Stat. Soc. B (1993) 3–23.
[63] I.M. Sobol, Uniformly distributed sequences with an additional uniform property, USSR Comput. Math. Math. Phys. 16 (5) (1976) 236–242.
[64] I. Sobol, B. Shukman, Random and quasirandom sequences: numerical estimates of uniformity of distribution, Math. Comput. Model. 18 (8) (1993) 39–45.
[65] G. GPy, A Gaussian Process Framework in python, 2012.
[66] J. Salvatier, T.V. Wiecki, C. Fonnesbeck, Probabilistic programming in python using pymc3, PeerJ Computer Science 2 (2016) e55.
[67] C. Si, X.-D. Wang, Z. Fan, Z.-H. Feng, B.-Y. Cao, Impacts of potential models on calculating the thermal conductivity of graphene using non-equilibrium molecular dynamics simulations, Int. J. Heat Mass Tran. 107 (2017) 450–460.
[68] L. Lindsay, D. Broido, Optimized tersoff and brenner empirical potential parameters for lattice dynamics and phonon thermal transport in carbon nanotubes and graphene, Phys. Rev. B 81 (20) (2010) 205441.
[69] J.-H. Zou, Z.-Q. Ye, B.-Y. Cao, Phonon thermal properties of graphene from molecular dynamics using different potentials, J. Chem. Phys. 145 (13) (2016) 134705.